The scintillator detector for the fast trigger and time-of-flight (TOF) measurement of the space experiment AMS-02

V. Bindi[a], D. Casadei[a,1], G. Castellini[b], F. Cindolo[c], A. Contin[a,*], F. Giovacchini[a,2], C. Guandalini[c], G. Laurenti[c], G. Levi[a], M. Lolli[c], L. Quadrani[a], F. Palmonari[a], C. Sbarra[a], A. Zichichi[a]

[a] Department of Physics and INFN, Viale B. Pichat 4/2, I-40127 Bologna, Italy
[b] CNR IROE, I-50125 Florence, Italy
[c] INFN of Bologna, Viale B. Pichat 4/2, I-40127 Bologna, Italy

Abstract

The "Time-Of-Flight" (TOF) system of the AMS-02 superconducting spectrometer, to be installed in the ISS International Space Station, consists of four layers of plastic scintillation counters. During the precursor mission AMS-01 (June 1998), a similar system successfully operated in space for 10 days. However, the AMS-02 TOF had to be redesigned taking into account the more stringent mass and power constraints of the AMS-02 detector. The main characteristics of the new TOF system are (a) capability to stand the high fringing field of AMS-02 superconducting magnet; (b) high redundancy of electronic components for unmanned operation of at least three years in the space station; (c) capability to operate in the space environment on the ISS. Counters and electronics have been extensively tested before the installation in the spectrometer.
Keywords: AMS experiment, Plastic scintillator, Time-of-flight, Cosmic rays

1 Introduction

The AMS-02 cosmic ray detector is the final achievement of an international collaboration started in 1994 [1] by S.C.C. Ting with the support of A. Zichichi, which presently includes 500 physicists from 60 research institutes in 16 countries.

AMS-02 is an improved version of the AMS-01 space spectrometer, which flew on the shuttle Discovery (NASA mission STS-91) in June 1998. AMS-01 took data for about 90 h at different flight altitudes, from 320 km to 390 km with latitude ranging within $\pm 51.7^\circ$ and all longitudes [2].

Figure 1 shows a schematic view of the AMS-02 detector.

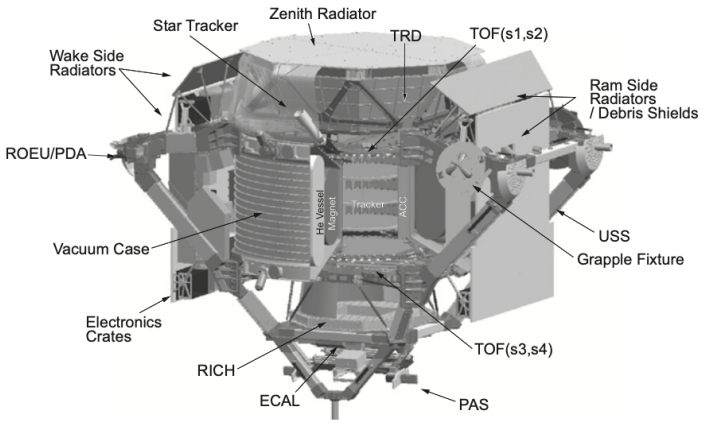

Fig. 1. The AMS-02 detector.

Figure 1: Schematic view of the AMS-02 detector.

Figure 2 shows the AMS-02 superconducting magnet.

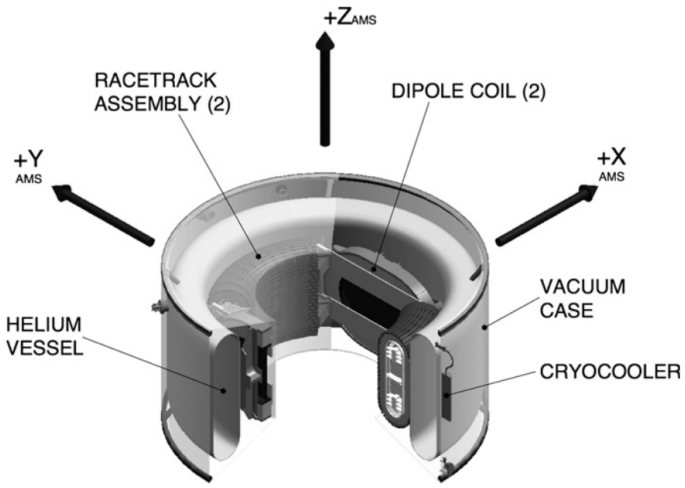

Fig. 2. The AMS-02 superconducting magnet.

Figure 2: The AMS-02 superconducting magnet.

The 0.8 T dipole field of the superconducting magnet has an intensity of about 6 times larger than the permanent magnet of AMS-01, with a residual magnetic field (< 15.2 mT at 2.3 m) and a dipole moment well below the ones allowed by the International Space Station (ISS) safety requests, thanks to the "racetrack" coils. The magnet operates at a temperature of 1.8 K cooled by superfluid Helium stored in a 2500 L vessel, which should serve a three years lifetime to the experiment. The silicon tracker has a larger surface than in AMS-01 and two more planes (eight in total). Its space resolution has been improved to 10 µm to be able to measure rigidities in the TV range.

The tracker measures the particle charge and the trajectory curvature which, together with the knowledge of the magnetic field intensity, provides an estimate of the particle momentum. The direction of motion, measured by the TOF system, is then used to determine the sign of the charge, an essential step to separate matter from antimatter particles. Finally, the anti-coincidence counters are used to veto all events in which particles enter the detector from a side, to avoid fake antimatter tracks originating by secondary particles produced by the interaction with the detector envelope.

To improve redundancy and particle identification, the following detectors have been installed on AMS-02:

- A transition radiation detector (TRD) which provides an electron/hadron separation of 10^3 at 20 GeV momentum, down to 10^2 at 300 GeV;
- A ring-imaging Cherenkov system (RICH) which provides a velocity resolution of 0.1 % for $Z > 1$ nuclei, up to about 10 GeV/n, and measures the particle charge up to Fe;
- An electromagnetic calorimeter (ECAL), 16 radiation lengths thick, which measures electromagnetic particles with a 2 % energy resolution at high energy and provides the electron/hadron rejection factor exceeding 10^3.

The expected performances and the powerful particle identification capabilities of AMS-02 are illustrated in Table 1, which shows the expected flux of cosmic rays detected in three years of data taking on board of the International Space Station.

Table 1: Monte Carlo expected number of cosmic ray particles in the AMS-02 acceptance above given energy thresholds in three years of data taking on the ISS.

	¿1 GeV/c	**¿10 GeV/c**	**¿10^2 GeV/c**	**¿1 TeV/c**
P	6.1×10^8	1.5×10^8	2.5×10^6	6.1×10^8
e^+	1.4×10^8	6.8×10^6	7.2×10^4	4.4×10^2
e^-	9×10^6	3×10^5	1.6×10^3	6
P (bar)	1.4×10^8	6.8×10^6	7.2×10^4	4.4×10^2
He	6.4×10^8	2.1×10^8	7.3×10^6	1.7×10^5

2 Design considerations

The AMS-02 TOF system is based on previous experience and well-established techniques [3, 4, 5, 6]. It has been completely designed and built at the INFN Laboratories in Bologna, to provide:

- The fast trigger to the experiment;
- Measurement of time-of-flight with resolution sufficient to distinguish upward from downward going particles at $\geq 10^{-10}$ level, and anti-protons from electrons up to $\sim$1.2 GeV;
- Measurement of primary cosmic nuclei velocity with $\sim$% resolution, and absolute charge up to $Z \approx 15$.

2.1 Key design parameters

Sensitive area: AMS-02 has been designed to have a large acceptance for cosmic ray tracks. The superconducting magnet aperture is about 0.4 m^2 sr, in order to reach a 10^{-9} sensitivity for the flux of anti-Helium/Helium nuclei, in one year of running. To match the full acceptance of the magnet, each layer of the TOF system has to cover a circular area of about 1.6 m^2.

Trigger selection: The TOF system has to provide the fast trigger to the AMS experiment. It consists of two planes of scintillator paddles mounted inside AMS-02. Each plane contains two layers of counters, in x and y directions, respectively. The first plane is situated at the entrance of the magnetic volume, the second one at the exit, at a distance of $\pm$626 mm in the z direction, as defined in the reference frame of the experiment. Each layer is made by $8-10$ scintillator paddles of different lengths, staggered by 1.5 cm in z and overlapped by 0.5 cm to avoid geometrical inefficiencies.

Weight: Given the strong limitations in the total weight of the AMS detector, the TOF system was allotted 268 kg to accommodate for the detector itself and for the support structure.

Power consumption: The TOF system was allowed to use about 150 W for photomultiplier tube operation and signal read-out, out of the 2 kW electric power given by NASA to the AMS experiment on the ISS.

Time-of-flight resolution: A resolution in the TOF better than 180 ps is needed to satisfy the physics requirements. The choice was one centimeter thick scintillator, as a compromise between the minimum thickness and the light output needed to reach this resolution.

A number of technical constraints had to be taken into account in designing the detector to ensure the performances previously described. The TOF system must tolerate the high mechanical stresses during the launch phase without breaking or damaging any part of the detector. Moreover, it must survive for at least five years in the harsh space environment, the main threats being the large temperature changes depending on the ISS orbits and attitudes, and the possible impact with micrometeorites and mini debris.

To accomplish all that, the counters are housed in mechanically robust and light-tight covers with a system for fast depressurization, supported by a structure conforming to the NASA specifications for Shuttle payloads about resistance to load and vibrations. The use of composite materials allows to keep the weight low.

To ensure that the system remains inside the permitted range of temperatures, a complete thermal analysis of the system, alone and coupled with the rest of the experiment has been performed. A complex system of active radiators have been installed, to keep the overall temperature and that of the single detectors within the defined limits.

The long term operational reliability of the TOF system is assured by its modular design. Every counter is read at both sides by at least two photomultiplier tubes and it can still trigger with only one

tube working. The same is true for the (unlikely) complete failure of one counter, as the normal trigger logic requires a signal in three layers out of four. In this way, the system is fault tolerant and somewhat redundant by design.

The powering and read-out electronics [7] are protected with conformal coating from the highly ionizing low-orbit space environment and passed qualification tests to verify the absence of sparks, discharges or leakage. The one per one redundant design ensures constant operation even in case of a hardware failure in the power supplies or in the read-out electronics.

3 The light detectors

The Photo-Multiplier Tubes (PMTs) used to collect the light from the TOF scintillators should operate in the strong (2 kG to 3 kG) fringing field of the superconducting dipole magnet [8]. Figure 3 shows the magnetic field magnitude at the vertical coordinate where the TOF planes are positioned.

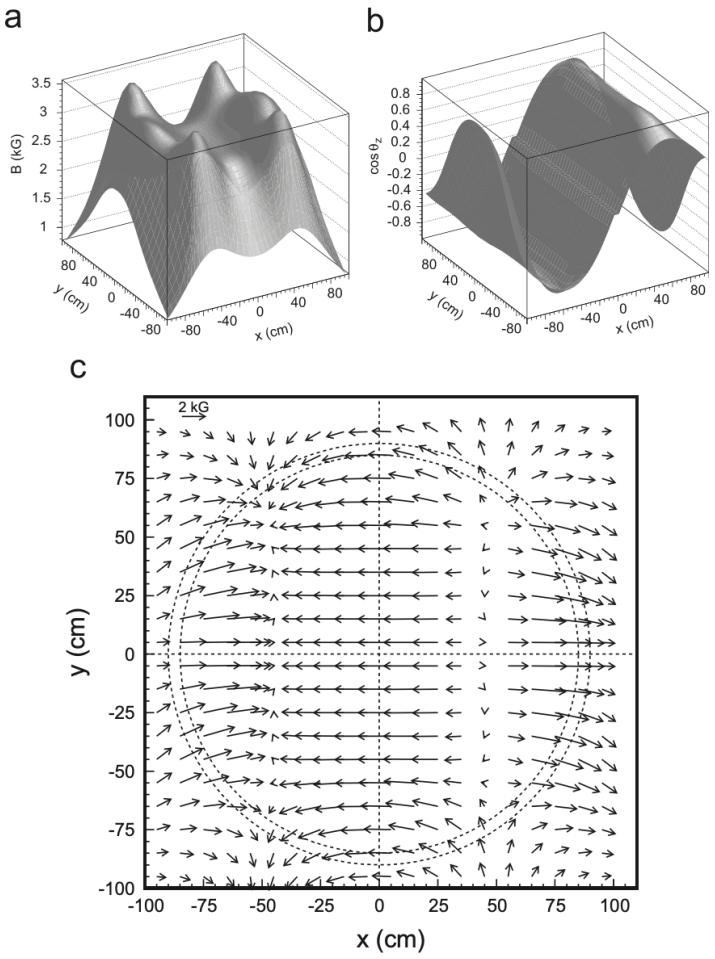

Figure 3: (a) Magnetic field magnitude, (b) direction w.r.t. z-axis, (c) (x, y) component at $z = 60$ cm. Dashed circles show PMT positions.

Because of the field magnitude, and of weight limits, the PMTs must withstand the magnetic field without shielding. The choice was fine-mesh PMTs, RS946 W/FL Hamamatsu (see Fig. 4), for their capability of working in high magnetic fields, while keeping good timing characteristics [9]. With a 16 mesh dynode chain, the gain is 10^6 at 2000 V, the rise time 1.9 ns, the transit time 7.7 ns and the single electron time jitter 0.35 ns at zero magnetic field.

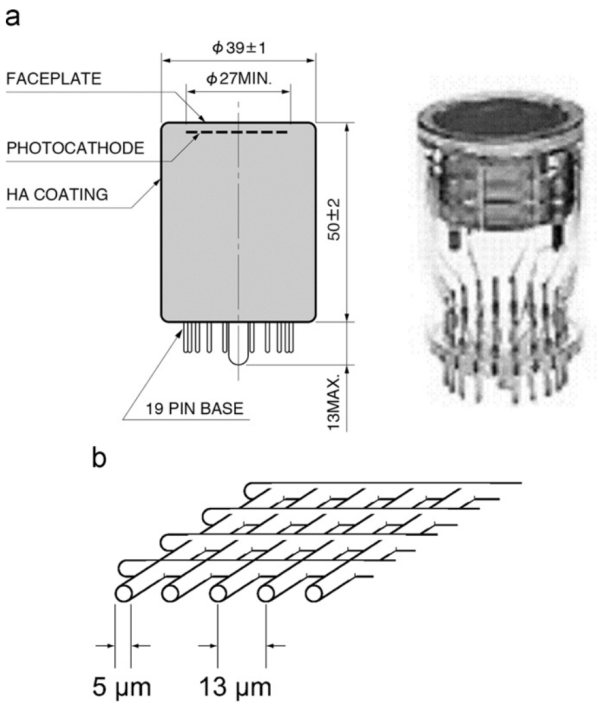

Figure 4: Fine-mesh Hamamatsu RS946 PMT: (a) compact assembly of the 16 meshes, 0.9 mm spaced (dimensions in mm); (b) mesh structure of a dynode.

3.1 Behavior in magnetic field

The RS946 Hamamatsu PMTs have been used for calorimetric applications in large experiments (e.g. the KLOE calorimeter [10]), whereas in the TOF apparatus the main task is to give an accurate timing of scintillation light pulses. For this reason the RS946 PMT behavior in magnetic field has been extensively studied, both in time resolution and pulse height response. To understand and validate the results of the measurements, a model simulation was also implemented that reproduces the single photoelectron spectrum and the amplitude and time response as a function of the intensity of the magnetic field and of its angle with respect to the PMT axis [11, 12].

The simulation results agree well with data. In particular, the probability that an electron hits the first dynode mesh increases at angles between the PMT axis and the magnetic field greater than 0° and below 40°, resulting in a larger PMT response. Above about 50° the electrons do not reach the first dynode and the PMT response decreases dramatically, as shown in Fig. 5.

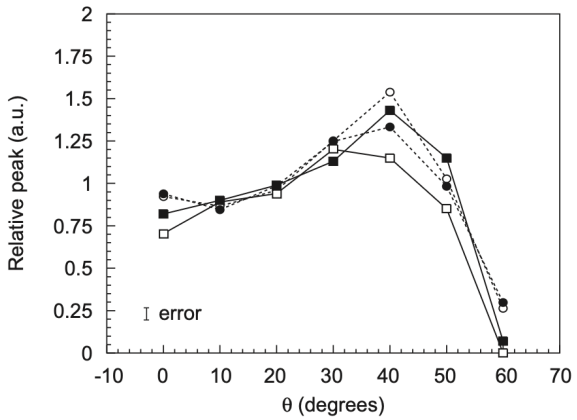

Figure 5: Measured (solid lines, squares) and simulated (dotted lines, points) relative gain as a function of the angle between the PMT axis and the magnetic field, at two values of magnetic field: 1500 G (black) and 3000 G (open) [12].

Due to the increase in flight path length of the electrons spiraling around the magnetic field lines, the jitter in transit time of the electrons from the photocathode to the first dynode increases with increasing angles between the PMT axis and the magnetic field and with increasing magnetic field, as shown in Fig. 6, where the contribution of the magnetic field has been obtained by subtracting in quadrature the jitter in transit time at zero field. This effect has been shown to be more critical for PMTs working at a lower voltage [12]. For the TOF of AMS-02 the strategy has been to increase the HV of the PMTs that are to be placed in the critical positions associated with highest angles with respect to the magnetic field.

The main expected effect of the magnetic field on TOF performances is a slight (about 10 %) worsening of the time-of-flight resolution of the overall detector.

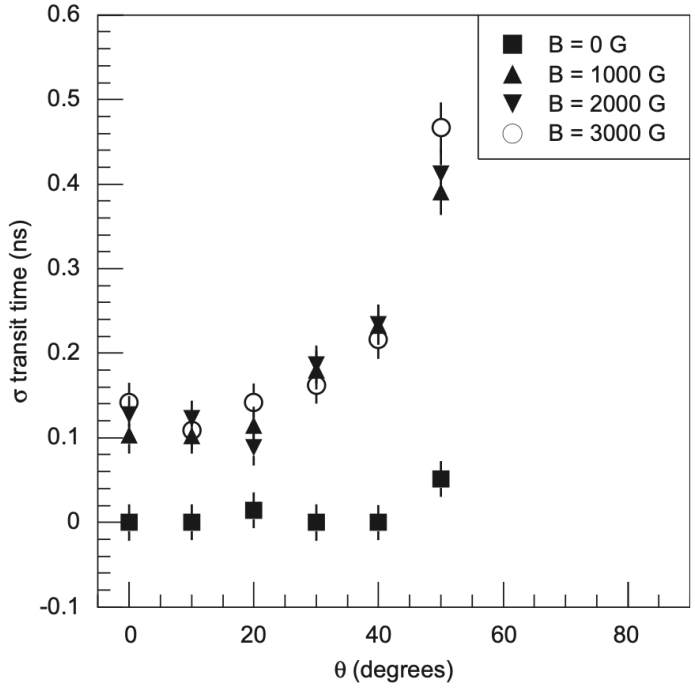

Figure 6: Contribution to the jitter in transit time of the magnetic field as a function of the angle between the PMT axis and the field, for different values of the magnetic field.

3.2 PMT thermal vacuum tests

The PMTs must withstand the severe space environmental conditions of the space station, namely low temperatures when facing open space and high temperatures when exposed to direct sun.

Extensive tests have been made in a thermal vacuum chamber built in Bologna, working at high vacuum and temperatures ranging from $-60\,^{\circ}$C to $120\,^{\circ}$C [13]. The tests were meant to verify the survival of the PMTs in the nominal range of temperatures specified by Hamamatsu. A group of 10 photomultipliers was tested at a pressure of about 10^{-6} mbar with temperature varying between $-30\,^{\circ}$C and $55\,^{\circ}$C. Four PMTs were equipped with a radioactive source and a small scintillator, used as a reference. Fig. 7 shows the variation of the pulse height as a function of temperature for two PMTs. Data are in good agreement with the PMT characteristics as given by Hamamatsu [9].

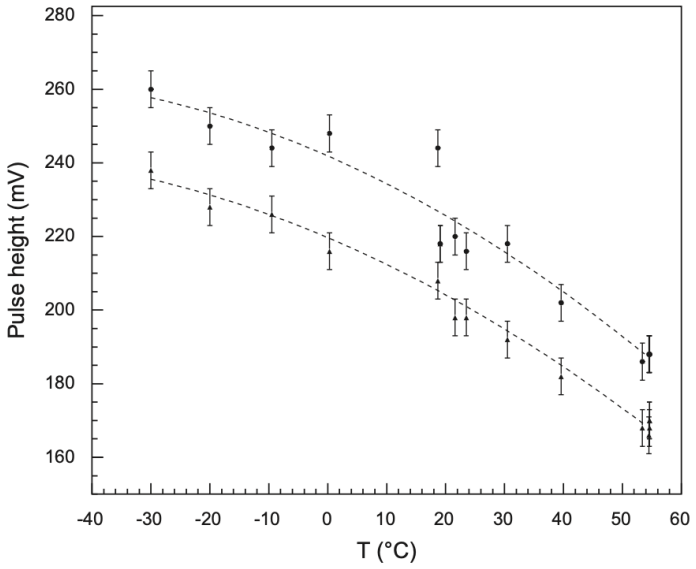

Figure 7: PMT response as a function of temperature. Dashed line: parabolic fit.

Other six PMTs were monitored for dark current at the same pressure and temperature range. Fig. 8 shows the variation of the dark current versus temperature for two PMTs. Even if an increase is clearly measured at high temperature, the dark current is always negligible.

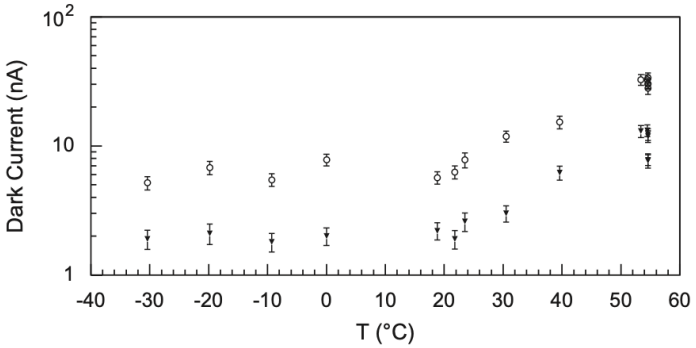

Figure 8: PMT dark current as a function of temperature.

4 The scintillation counters of the TOF detector

4.1 Design

Each counter of the TOF detector is made of a 1 cm thick scintillator paddle optically coupled at both ends with PMTs in order to have a time resolution nearly independent from the position of the impact point of the measured particle. Each paddle is read-out by two PMTs ($2 \times 5.7\,\mathrm{cm}^2$ cathode area) at each end, almost matching the area of the scintillator cross-section ($12\,\mathrm{cm}^2$), thus ensuring an efficient light collection. Mechanical constraints due to the superconducting magnet vacuum case and to the support structures of the other AMS-02 detectors required a different design for the upper TOF plane (UTOF—layers 1 and 2), mechanically connected to the TRD, and for the lower TOF plane (LTOF—layers 3 and 4) mechanically connected to the Unique Support Structure (USS).

As shown in Fig. 3, the angle between the counter axis and the magnetic field varies from about 0° to nearly 90°. On the other end, the maximum angle between the PMT axis and the magnetic field should be limited to less than 45° (see Section 3.1). The best orientation of each PMT, compatible with all the mechanical constraints, was therefore chosen for each PMT to conform to this limit.

Plexiglass light guides of different shapes consisting in complex strips accordingly tilted or twisted in function of the local magnetic field have been designed and built. Glued to them, conical light guides

couple each counter to the PMTs.

Round optical silicon (Dow Corning 93-500) rubber disks are used as optical contacts and mechanical pairing between the light guide and the PM photocathode window. An example of the design for one of the layer 2 counters is shown in Fig. 9.

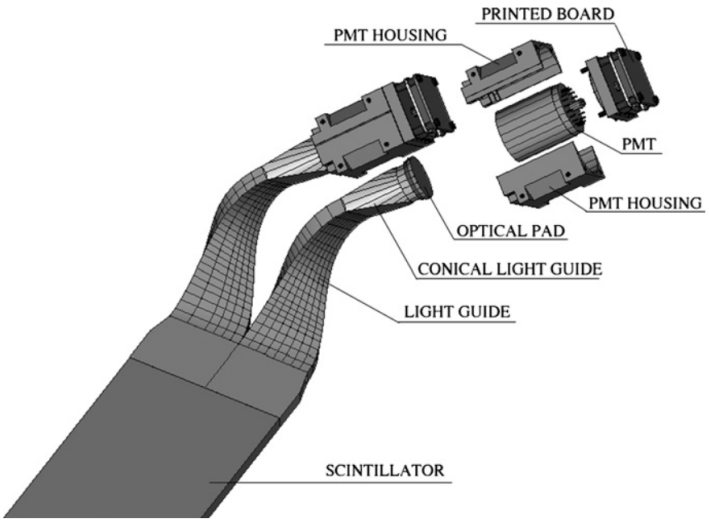

Figure 9: CAD picture showing the light guide shape needed to match a scintillator paddle to the PM oriented according to the magnetic field vector, and all other mechanical elements.

The resulting field amplitude and angle distribution with respect to the magnetic field for all PMTs are shown in Fig. 10.

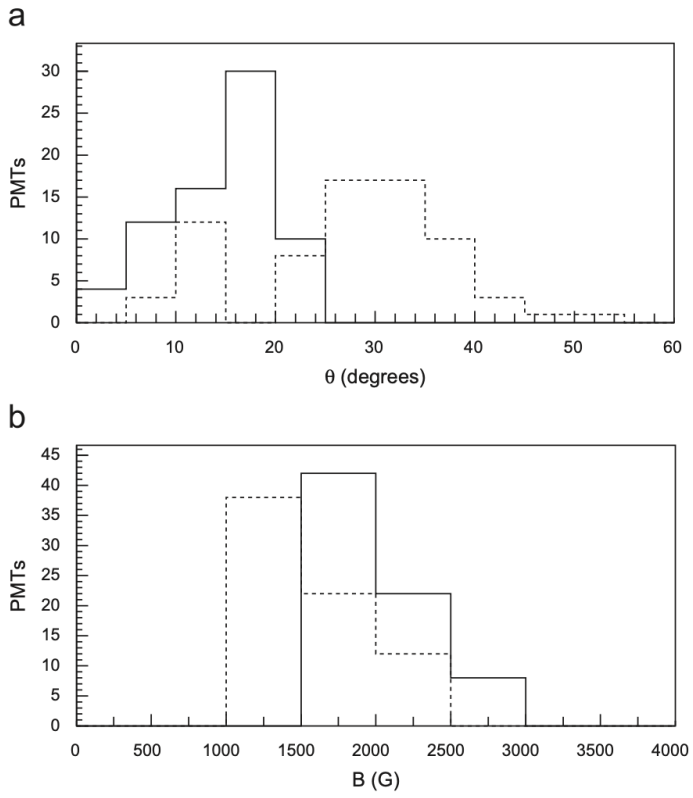

Figure 10: Magnetic field direction w.r.t. PMT axis (a) and intensity (b) distributions for all PMTs. Full lines: layers 1 and 4. Dotted lines: layers 2 and 3.

4.2 Counters assembly and test

In Figs. 11 and 12 the CAD top views of UTOF and LTOF detectors are shown. The total number of scintillation counters is 34, namely 8 in layers 1, 2 and 4, and 10 in layer 3.

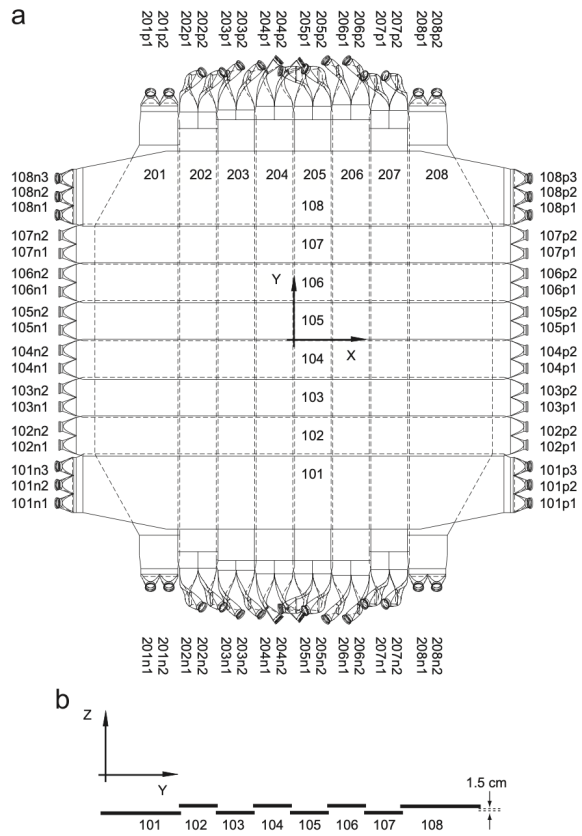

Figure 11: The $8 + 8$ scintillator counters and light guides CAD design for the UTOF detector. (a) Top view; (b) side view of layer 1.

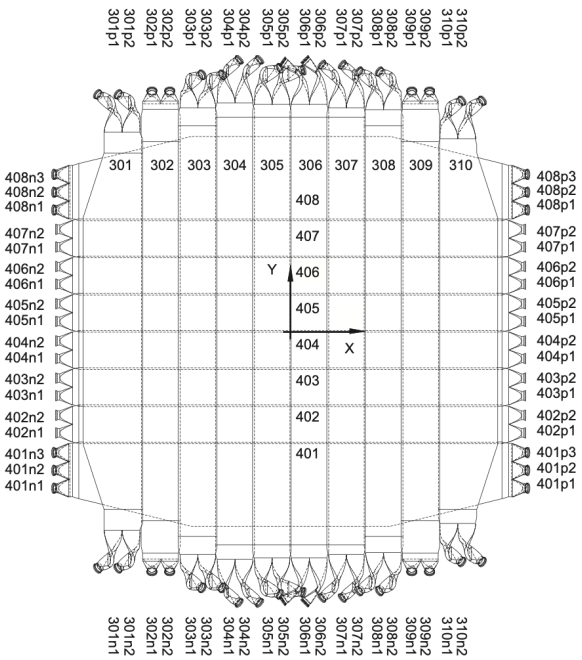

Figure 12: The $10 + 8$ scintillator counters and light guides CAD design for the LTOF detector.

4.2.1 Plastic scintillators and light guide assembly

The scintillator material is Eljen Technology EJ-200, widely used in large dimension detectors for the low attenuation of light and fast time response (0.9 ns rise and 2.1 ns decay times). It was delivered already cut at the required dimensions with the edges properly polished for maximum reflectivity and the end borders prepared for glueing.

Maximum effort was done to minimize the number of different types of counter and to provide for each type at least one spare. In Table 2 the different counter types are listed. All counters, once assembled with the light guides, have been wrapped with aluminized mylar and enclosed in a rigid carbon fiber box. All counters have been tested in a cosmic ray test telescope, using the same photomultipliers and the same electronics for all of them. From the pulse height spectrum of particles hitting the center ($\pm 3\,\mathrm{cm}$) of the counter, the total number of photoelectrons collected at both sides of the counter was evaluated as

$$N_{\mathrm{ph}} = \frac{1}{\sigma_{\mathrm{g}}^2} \quad \text{with} \quad R = \frac{Q_{\mathrm{n}} - Q_{\mathrm{p}}}{Q_{\mathrm{n}} + Q_{\mathrm{p}}}$$

where Q_{n} and Q_{p} are the signal amplitudes seen at side n and p of the counter, respectively, and σ_{g}^2 is the variance of the R distribution.

The results of this first calibration show that the average number of photoelectrons decreases for the more complex light guides, as shown in Fig. 13.

The light transmission efficiency of the 10 different light guide types was also simulated with a ray tracing program taking into account the angular distribution at the light guide entrance and the angular acceptance on the cathode glass window. The results, shown in the last column of Table 2, agree well with the measurements shown in Fig. 13.

Table 2: Counter types with light guide shapes and simulated efficiencies.

Counters	**Light guide**	**Shape**	**Length (cm)**	**Sim. eff. (%)**
102–107	Straight	Rectangular	130.5	84.9
402–407	Straight	Rectangular	134.0	84.9
202,303	Tilted	Rectangular	127.0	62.1
204,305	Tilted	Rectangular	132.2	64.6
302,309	Tilted	Rectangular	117.2	74.2
203,304	Tilted/twisted	Rectangular	132.2	63.1
206,307	Tilted/twisted	Rectangular	132.2	65.6
205,306	Tilted/twisted	Rectangular	132.2	62.1
207,308	Tilted/twisted	Rectangular	127.0	63.9
101,108	Tilted	Trapezoidal	126.5	48.5
401,408	Tilted	Trapezoidal	130.0	48.5
201,208	Tilted	Trapezoidal	117.2	64.6
301	Tilted/twisted	Trapezoidal	110.0	64.6
310	Tilted/twisted	Trapezoidal	110.0	64.6

For the trapezoidal counters, the simulation took into account also the counter geometry, therefore the efficiency is much smaller than for the rectangular counters.

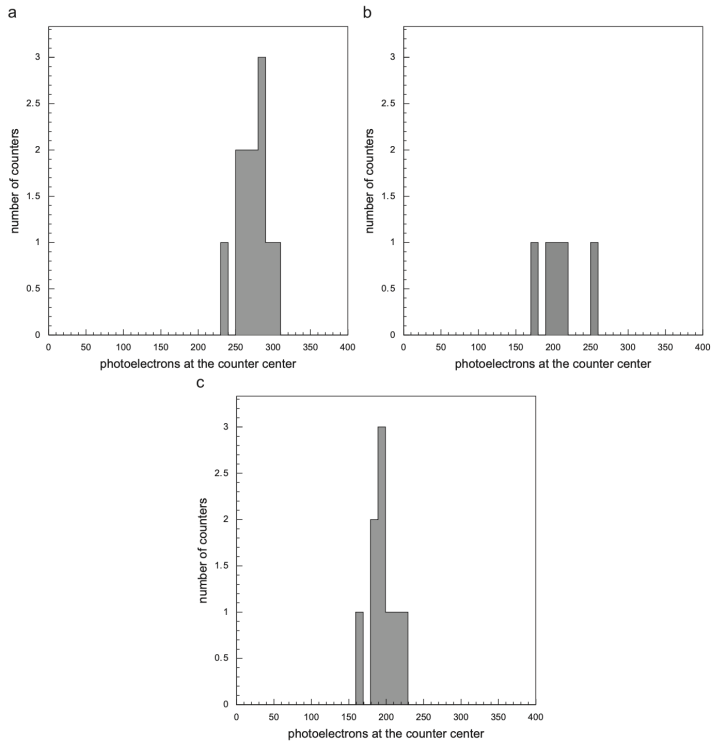

Figure 13: Distribution of the number of photoelectrons for counters with (a) straight, (b) tilted, and (c) tilted and twisted light guides.

4.2.2 Plastic scintillation counters assembly

The next step was to equip each counter with photomultipliers, test them in vacuum for proper high voltage insulation of the PMT base and of the flight cables and study their response to particles in the cosmic ray telescope.

PMTs should in principle be operated independently from each other. However, due to weight and power limitations, each high voltage (HV) channel was set to power two PMTs. To increase the fault tolerance of each side of the counter, the two PMTs on the same side are powered by different HV channels. The best combination of PMTs was determined with a "simulated annealing" algorithm (checked with a genetic algorithm) [14] in order to have equal HV on both PMTs in the same side. This guarantees similar photoelectron transit time and hence time resolution.

The assembly of the PMT electronics is shown in Fig. 14. The PMT flying leads are soldered to the first card of the base and connected via a kapton cable to a second card holding the HV divider resistor and capacitors on one side, and the HV shielded cable, the anode and dynode 50 Ohm cables on the other side. The first card is potted to the glass PMT shocklet, the second is suitably coated to ensure electrical insulation. A grounding card which mechanically protects the whole base is finally added. The anode signals from the PMTs on each side of the counter are passively summed to be used at the trigger level and to measure low charged particles (up to $Z = 4$). The third last dynode of each PMT is read-out independently, through electronics cards mounted inside the detector covers, to measure higher charges (up to $Z = 15$).

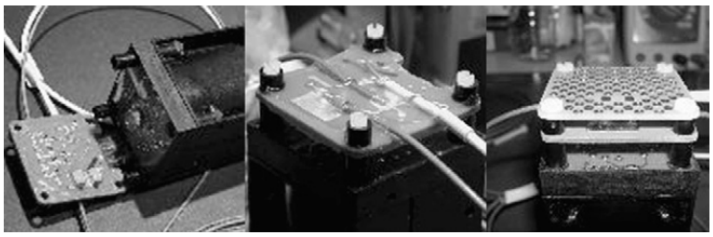

Figure 14: PMT base assembly: (left) second card opened showing HV divider; (center) second card closed with cables; (right) third card with ground plane.

The PMT bases were then mounted on the light guides and covered with a thin copper electromagnetic shield, as shown in Fig. 15.

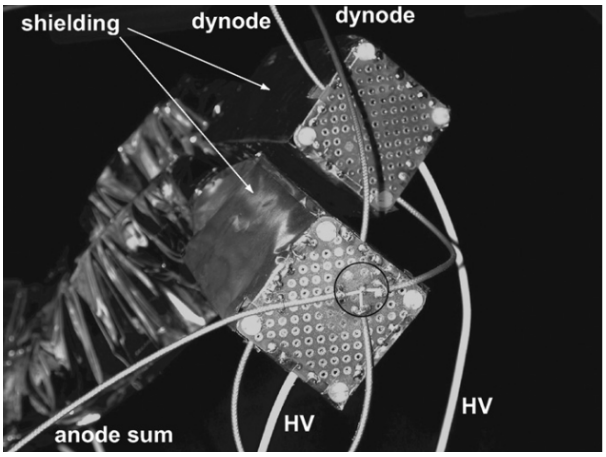

Figure 15: Final PMT mounting with electromagnetic shielding and signal/HV cables. The anode sum is indicated by the black circle.

The following characteristics of each counter were measured using cosmic rays:

- Attenuation lengths measured at both ends ($\lambda_{\rm on}$ and $\lambda_{\rm op}$);
- Light velocity in the scintillator;
- Number of photons at the counter center;
- Intrinsic time resolution (half difference of times from the two sides);
- TOF resolution (relative to a reference counter).

As an example, the results for the eight counters of layer 1 of upper TOF are shown in Figs. 16–18. A typical attenuation length is 150 cm (Fig. 16), the number of photoelectrons for straight light guides is about 260 (Fig. 17) and the effective velocity of light propagation along the scintillator is about 14 cm/ns (Fig. 18).

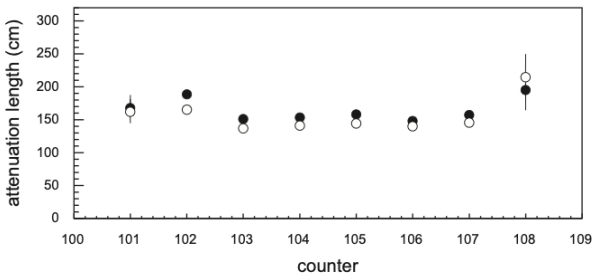

Figure 16: Attenuation length for layer 1 counters on side p (black) and side n (open).

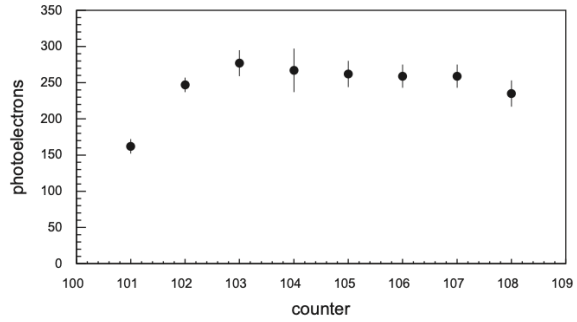

Figure 17: Photoelectrons produced at counter center for layer 1 counters.

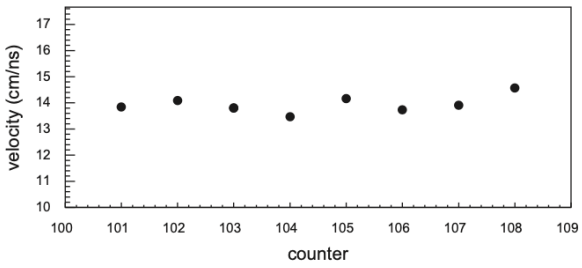

Figure 18: Effective light velocity for layer 1 counters.

Fig. 19 shows the time resolution as a function of the hit position of the particle, for a counter with straight light guides (120 ps to 150 ps), and for one with tilted and twisted light guides (150 ps to 200 ps), respectively. The lower number of collected photoelectrons in the latter determines a larger time resolution, as expected.

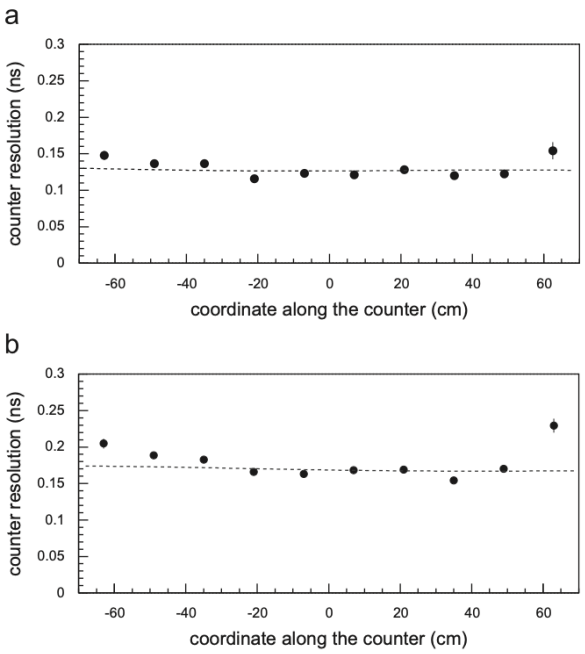

Figure 19: Time resolution along the counter for (a) straight light guides and (b) tilted/twisted light guides.

5 Test beam results

Two AMS-02 TOF counters, together with one AMS-01 counter used as reference, have been tested with a Pb beam at 20 GeV/c/amu, accelerated by the Super Proton Synchrotron (SPS) at CERN and colliding with a Be target [15]. The secondary fragments (all nuclei up to Pb, mostly with the same momentum per nucleon as the primary beam) were filtered through the H8 selection line, obtaining a 3 cm^2 ion beam with given A/Z ratio (i.e. defined rigidity). The selection line was set at values $A/Z = 2, 3/2, 7/4$ and 1 to have similar rates for all ions.

Fig. 20 shows the peak response of the counters to various ions. The energy loss dE/dx by a particle with atomic number Z is proportional to Z^2, but the emitted scintillation light is proportional to dE/dx only for small values of the energy loss. In general, the amplitude Q of the signal is the time integral of the PMT current pulse, i.e. it is proportional to the emitted scintillation light, and can be written as

$$Q = \frac{aZ^2}{1 + bZ^2 + cZ^4}$$

according to Birks' formula [16].

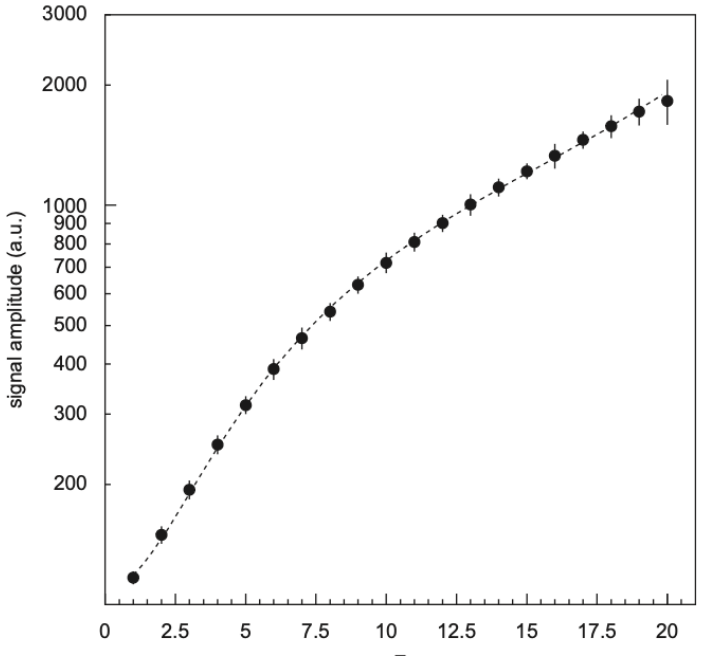

Figure 20: Signal amplitude as function of particle charge. Dashed line: Birks' law fit.

The amplitude spectra for different ions have then been corrected for the scintillator response. The result is shown in Fig. 21.

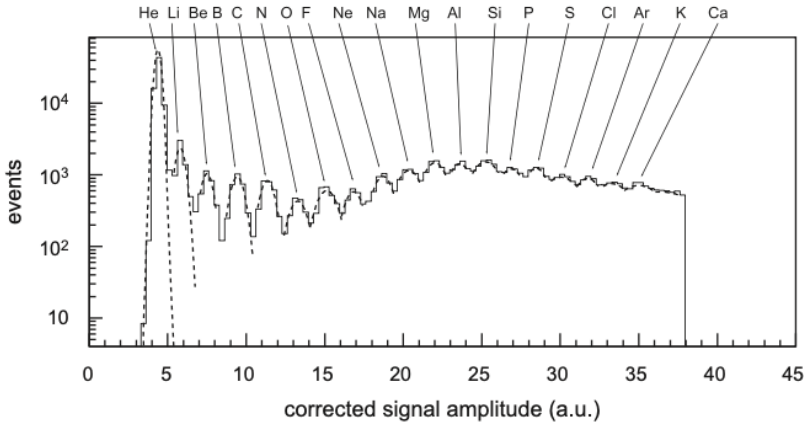

Figure 21: Detector response, corrected for saturation, as function of ion charge. Dashed lines: Gaussian fits.

The charge resolution of a single counter, shown in Fig. 22, degrades with an increasing charge, as expected given the saturation of the emitted light. In AMS-02 the charge resolution is expected to improve by a factor two, using four independent measurements of the energy deposited by the particle in the four TOF layers. Therefore, the complete TOF detector should allow ion identification up to charge $Z \approx 15$.

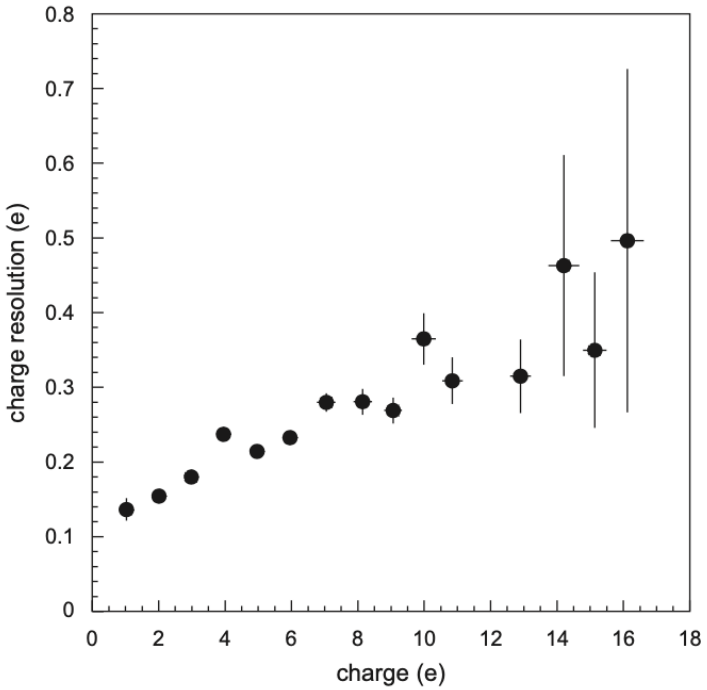

Figure 22: Charge resolution of single counter response, corrected for saturation.

The time-of-flight resolution, measured between the two AMS-02 counters and shown in Fig. 23, decreases with increasing Z, following the formula:

$$\sigma_t = \sqrt{\left(\frac{P_1}{Z}\right)^2 + P_2^2}, \quad P_1 = 159(2)\,\text{ps},\ P_2 = 79(1)\,\text{ps}$$

The first term in the resolution is inversely proportional to Z and hence to the square root of the number of photoelectrons produced by the particle; the second term is a constant representing the overall time resolution of the electronics chain (including cables).

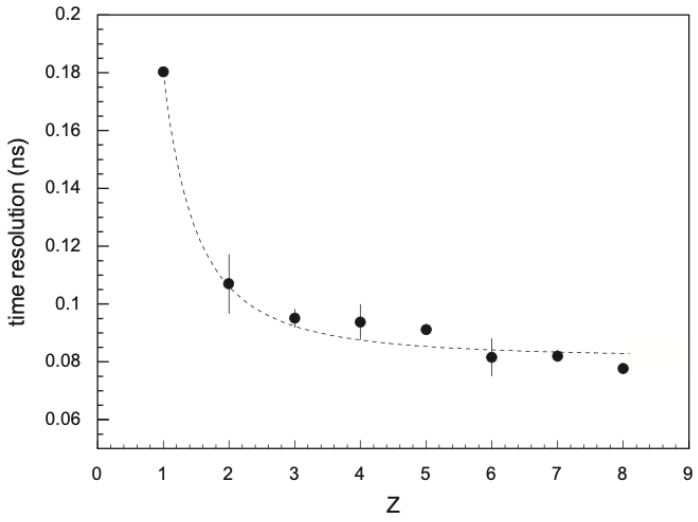

Figure 23: Time resolution as function of ion charge. Dashed line: fit to data.

6 The LTOF and UTOF detectors assembly

The mechanical supports for TOF planes are designed to be accommodated into the general mechanical structure of AMS-02. They have been calculated through structural and modal analysis, to sustain the acceleration and vibration stresses induced during the early stage of the Space Shuttle take-off and to define the eigenfrequencies of the overall systems. Vibrational and TVT tests on prototypes of single sub-assembly or parts were performed at an early phase of the design to validate it. Special care was used to ensure that PMTs could stand the induced stresses. The supporting structure has been consequently designed to minimize them.

Figs. 24 and 25 show the exploded view of the mechanical structure of upper and lower TOF, respectively.

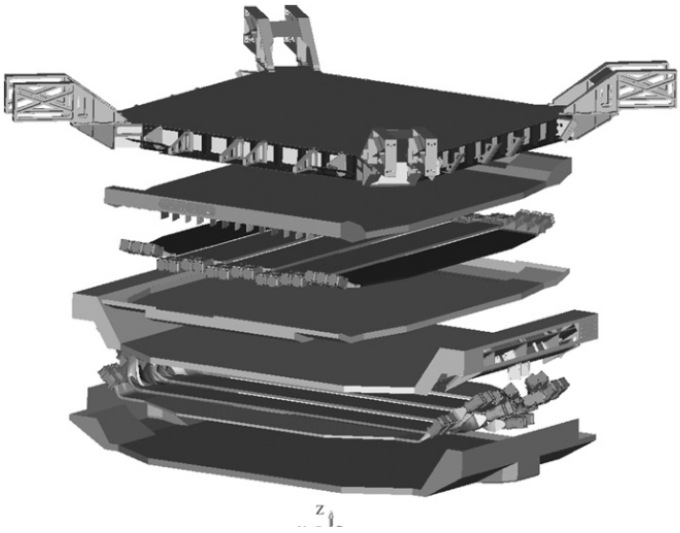

Figure 24: Exploded view of the UTOF assembly.

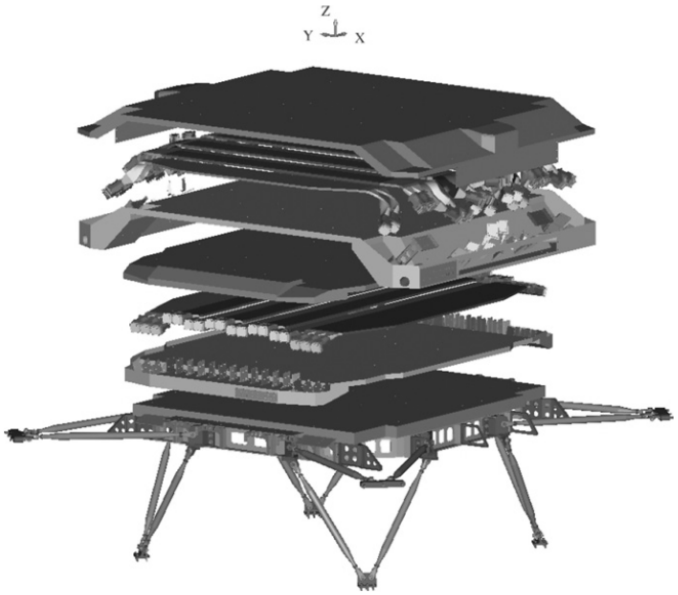

Fig. 25. Exploded view of the LTOF assembly.

Figure 25: Exploded view of the LTOF assembly.

A rigid aluminum honeycomb plate is used as a general support structure attached to the USS. Light aluminized carbon fiber covers enclose each layer, ensuring the necessary light tightness and providing an electromagnetic shielding. Each counter inside the box is in turn fixed to the covers and to the honeycomb plate by means of special carbon fiber brackets. The same has been done for the PMTs at the two ends of the counters. A special soft open cell rubber foam is placed between the counters to dump the effect of vibrational modes.

The honeycomb support of UTOF is 10 cm thick, reinforced by aluminum beams around the perimeter and rigidly connected to the TRD support structure. The honeycomb support of LTOF is 5 cm thick and reinforced by an octagonal aluminum structure connected to it. It is fixed vertically by 16 tension rods to the USS.

In Table 3 the thickness of material traversed by particles is reported for UTOF and LTOF. The minimum thickness for a particle traversing the spectrometer with normal incidence (bold characters in Table 3) is 6.72 g/cm^2 or 18.05 % of a radiation length. The thickness traversed by particles, including the filling foam which covers about 50 % of the sensitive area, and the thickness for particles traversing all counter fixtures, covering 4 % of the sensitive area, are displayed in the last rows. Notice that the probability of traversing this maximum thickness is less than 0.2 %.

Table 3: TOF detector thicknesses.

	Thickness (g/cm^2)		**Radiation lengths (%)**	
Element	**UTOF**	**LTOF**	**UTOF**	**LTOF**
Plastic scintillator (2 × 1 cm)	2.06	2.06	4.7	4.7
Counter cover (4 × 1 mm carbon)	0.23	0.23	0.5	0.5
Layer support (4 × 0.7 mm carbon)	0.32	0.32	0.7	0.7
Detector support (Al honeycomb)	0.71	0.75	2.95	3.3
gray!10 **Minimum thickness**	**3.40**	**3.32**	**9.2**	**8.85**
Filling foam (15 mm rohacell)	0.32	0.32	0.7	0.7
Total thickness (50 % area)	3.72	3.64	9.9	9.55
Counter fixtures (18 mm carbon)	2.15	2.15	4.7	4.7
Total thickness (4 % area)	5.87	5.74	14.6	14.25

7 Space qualification tests

Space qualification of the detector is required by NASA in order to satisfy the safety conditions for payloads using the Space Shuttle (Vibration Tests—VTs), and to verify its functioning in space conditions

(Thermal Vacuum Test—TVT).

The TVT consists in several thermal cycles in a vacuum chamber reproducing the temperature range and the pressure of AMS when operated on the ISS. The VTs consist in dynamic mechanical tests on vibrating tables simulating the Shuttle during take-off. Both tests, executed separately for LTOF and UTOF, have been performed at the SERMS Laboratories in Terni (Italy) with the supervision of Carlo Gavazzi Space.

7.1 Thermal vacuum test

During TVT (Fig. 26) the detector underwent four thermal cycles at the pressure of about 3×10^{-5} mbar. The maximum (minimum) temperature was 50 °C (−35 °C) with the detector switched off (non-operative) and 43 °C (−32 °C) with the detector switched on (operative). During the fourth cycle, a thermal balance (TB) was performed with the temperature stabilized for 5 h at the maximum (hot balance) and at the minimum (cold balance) operational temperatures (Fig. 27).

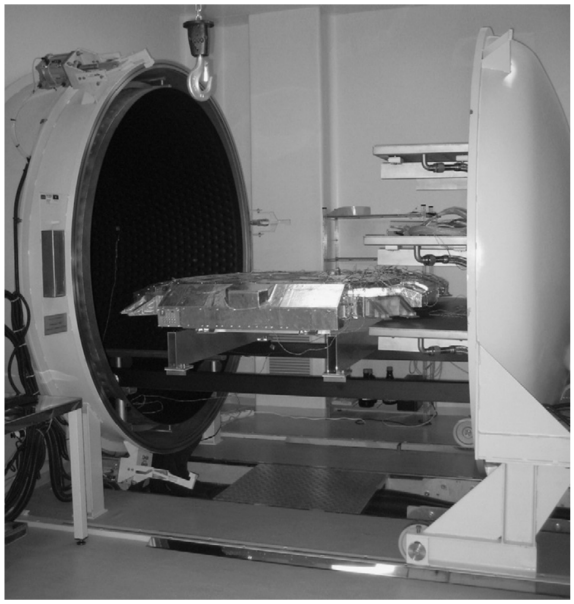

Figure 26: Upper TOF being inserted into the thermal vacuum chamber at SERMS.

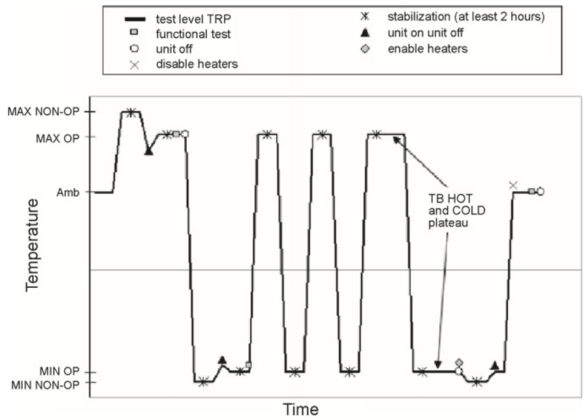

Figure 27: Temperature cycle for TOF thermal vacuum test. Thermal balance performed during fourth cycle.

The temperature was continuously monitored inside the detector by 32 Dallas sensors DS18S20 and on the outside by 44 PT100 sensors.

As a result of these tests, and following Hamamatsu specifications, the operating temperature range of the TOF detector has been fixed between $-30\,^{\circ}\mathrm{C}$ and $35\,^{\circ}\mathrm{C}$ and the non-operating temperature range between $-35\,^{\circ}\mathrm{C}$ and $42\,^{\circ}\mathrm{C}$. This temperature range is somehow larger than what is expected in space and should guarantee a safe operation of the system during several years.

During data taking in space, Dallas sensors (eight in each TOF layer) will continuously monitor the temperatures of the PMTs to verify that they stay within the limits. A system of heaters, powered independently from the ISS and activated by mechanical thermostats, will ensure that the detector temperature will not decrease below the lower limit in emergency conditions (e.g. in case of long-lasting power failure in the ISS). According to the thermal simulations, the temperature upper limit should never be reached when the detector is switched off. During operation of the detector, the PMTs will be switched off if the maximum allowed temperature is reached.

7.2 Vibration tests

Vibration tests (Figs. 28 and 29) were performed in order to verify that:

- The TOF first mode frequency was higher than 50 Hz;
- The TOF detector performances were not degraded by the Maximum Expected Flight Level (MEFL) vibration environment, as defined in Ref. [17].

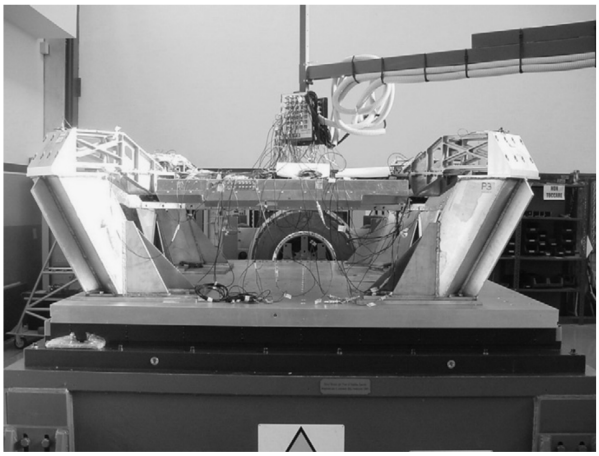

Figure 28: UTOF on sliding table during (x, y) plane vibration test.

Figure 29: LTOF on shaker during z-axis vibration test.

The VTs were performed along the three axes with a shaker and a sliding table. Two dedicated fixtures, one for the z axis and one for the (x, y) plane, were specially built for the purpose.

Accelerometers were used to monitor the detector during the vibration tests and to measure the local induced acceleration in different points. The accelerometers were positioned both inside and outside the detector. Pilot accelerometers were used to drive the shaking table and stop the test in case of excessive value.

First of all a search of the resonance frequencies of the fixtures and of the detector, separately, was carried out using the following parameters (sine input):

- Linear frequency scan band: 5 Hz to 2000 Hz
- Scan speed: 2 oct/min (sweep up only);
- Level: 0.3 g (peak); control: multipoint input control.

Then the full test of the detector was performed following the MEFL random spectrum: the random vibration started with a low level (-9dB) approaching gradually (-6dB, -3dB) the full level (0 dB). After the vibration test, a resonance search was repeated to verify that no frequency shift occurred.

As a result from the VTs, the following objectives have been verified: LTOF and UTOF survived the vibration environment without degradation. No discrepancies between resonance before and after each random vibration, no deformation, damage or loose parts were observed. The first mode of vibration for UTOF and LTOF confirmed the expectation of the mechanical models.

7.3 Functional tests

Functional tests of the detectors were performed before and during TVT, and before and after VTs.

The trigger to the data acquisition was given by the anode signals from the central counter of each layer. The amplitude of all the anode signals, the PMT power consumption and the Dallas sensor temperatures were acquired by custom electronics boards.

Data were recorded at each minimum and maximum operative temperature. Fig. 30 shows the relative amplitude in each layer as a function of the temperature. The TOF response increases at lower temperature and decreases at higher temperature with respect to the values measured at room temperature, as expected from the single PMT thermal vacuum tests (Section 3.2).

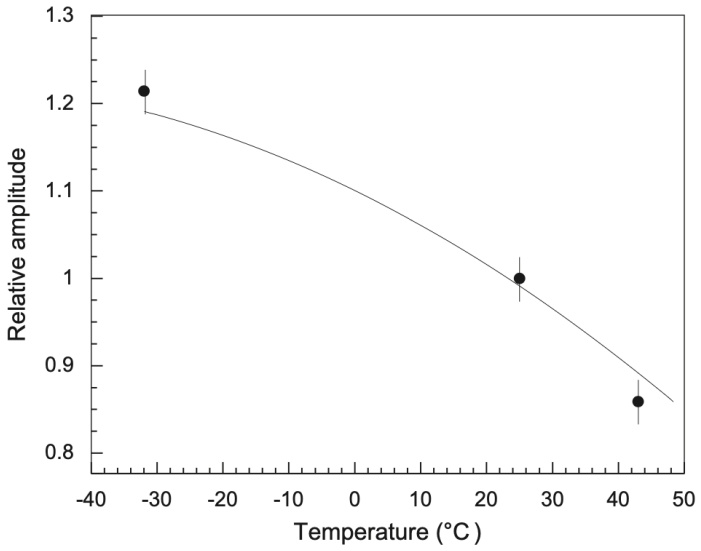

Figure 30: Anode amplitude at different temperatures relative to room temperature, averaged over all counters. Line: fit to PM response.

Before and after each vibration, data were recorded in order to check the detector functionality. In Fig. 31 the mean anode amplitude for each TOF layer after vibration, relative to the amplitude before TVT, is shown. Layers 1, 2 and 4 show a rather small decrease (about 10 %) of the response, compatible with the scintillator accelerated ageing due to the thermal stresses of the TVT test.

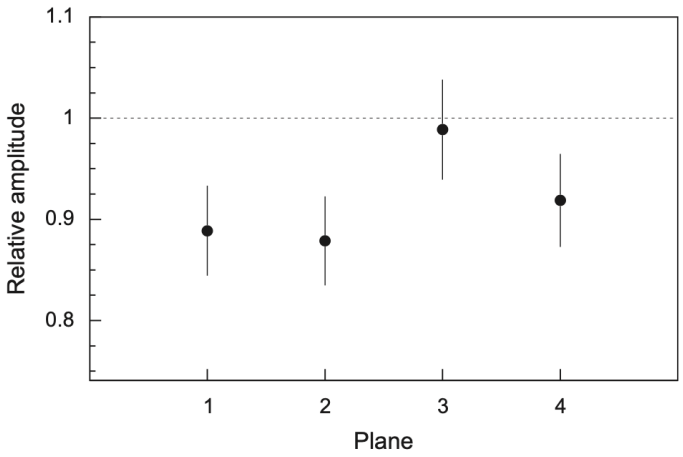

Figure 31: TOF layers anode amplitude after VTs, relative to before TVTs.

8 Final characterization before integration

Before being delivered to CERN for the integration in the AMS-02 spectrometer, the LTOF and UTOF detectors have been tested to verify that all counters were working properly, taking the last chance of making changes, in case some reparation was needed, just before the final sealing for mechanical and light tightness.

The main purpose of this characterization was the setting of the PMT high voltages and of the trigger thresholds. The performances of the full detector will be the subject of a subsequent paper.

Due to the powering scheme described in Section 4.2.2, two PMTs in different counters are paired to the same HV channel, but each counter must be able to operate with only one PMT powered in each side. Purposes of the test were:

1. To set the HV of each PMT so as to have a minimum ionizing particle signal passing a 60 mV threshold at the counter center, thus ensuring a good trigger efficiency in case of a failure of the other PMT on the same counter side, or of the corresponding HV line.

2. To set a HV value acceptable for both PMTs connected to the same HV channel. In case a PMT required a HV higher then the paired one, both have been set to the higher HV value.

3. To measure the performances of the counters using the HV set as in (2) for all channels.

After setting the HVs for each PMT with a standard threshold curve, data were taken by self-triggering the scintillation layers.

Data analysis gave a quite complete overview of the counters characteristics, as shown in the sample graphs reported in Figs. 32 and 33 which refer to counter 402 of layer 4. In this case the pulse heights at the center of the counter are not equal (see Fig. 32). However, the resolution for one minimum ionizing particle is the same, as expected, at about 15 %.

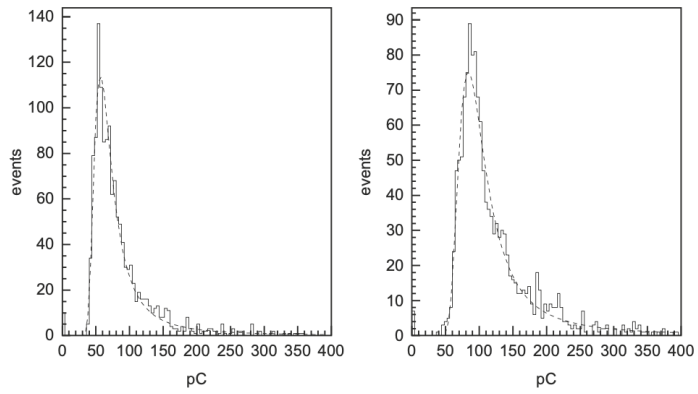

Figure 32: Anode pulse height spectra of sides n and p of counter 402 for events in 10 cm central section, fitted with Landau function.

The peak amplitudes of sides n and p are

$$Q_n(\Delta t) = Q_{n0}e^{\Delta t\nu/\lambda} \quad \text{and} \quad Q_p(\Delta t) = Q_{p0}e^{\Delta t\nu/\lambda}$$

where Q_{n0} and Q_{p0} are the peak amplitudes at the counter center, ν the velocity of light in the counter, λ the attenuation length and $\Delta t = (t_n - t_p)/2$ the time difference of the anode signals from the two sides of the counter, proportional to the hit position according to an effective light velocity ν of around 14 cm/ns.

Consequently, the straight line in Fig. 33 is

$$\log Q_n/Q_p = C_1 - C_2\Delta t$$

where $C_1 = \log Q_{n0}/Q_{p0}$ and $C_2 = -2\nu/\lambda$ are the parameters of the linear fit.

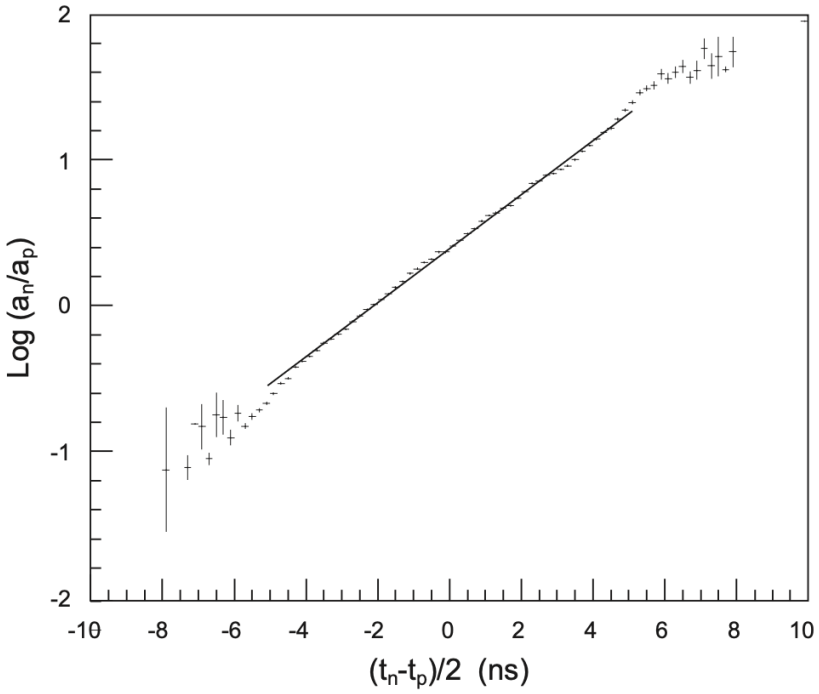

Figure 33: Counter 402: logarithmic ratio of pulse heights as function of arrival time difference. Straight line: linear fit.

Using a telescope of two scintillation counters, 10 cm wide by 140 cm long, 20 cm apart, which defined vertical cosmic muons and could be moved above the LTOF and UTOF detectors, the pulse height as a function of position of each counter was measured. Sample results are shown in Fig. 34.

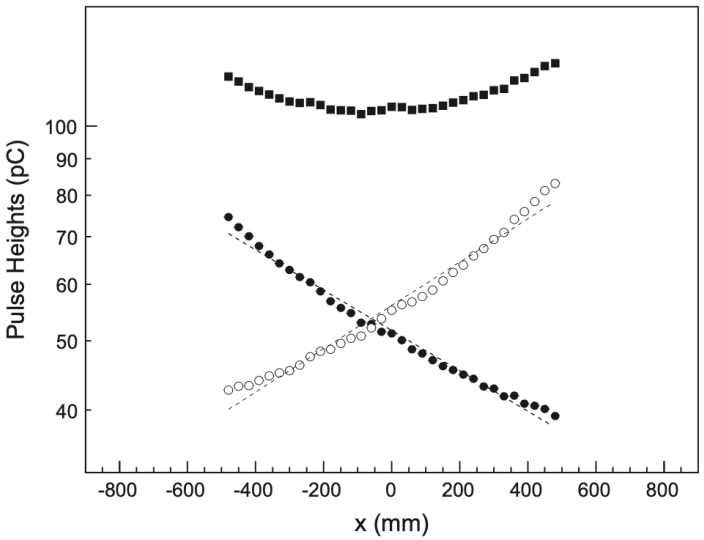

Figure 34: Counter 402: pulse height for MIPs vs. hit position; p side (white), n side (black) and sum (squares). Dashed lines: exponential fits.

9 Conclusion

The Time-Of-Flight system for the AMS-02 experiment and the associated electronics have been built according to the specifications. The main features of the system are:

- Large sensitive area: 6.4 m^2;
- Low power consumption: 150 W;
- Low weight: 264 kg;
- Fault tolerance in the read-out chain;
- Space-qualified according to NASA specifications.

A time resolution of the order of 160 ps for minimum ionizing, unit charge, particles can be anticipated, considering at least three layers hit. This corresponds to a resolution in β of 4 % at $\beta = 1$. For cosmic ray nuclei with $Z > 1$, the resolution approaches 2 %. This performance ensures an efficient rejection of upward-going nuclei, needed to search for antimatter in cosmic rays.

Ions can be identified up to charge $Z \approx 15$, thus complementing the measurements of the RICH and of the tracker.

The normal trigger configuration in space will require a hit on three TOF layers out of four, therefore the efficiency of each layer can be monitored during data taking. Moreover, dedicated (prescaled) trigger configurations will be used to monitor the overall trigger efficiency of the AMS-02 detector.

Note added in proof

Following March 11, 2010, NASA decision to extend the life span of the ISS beyond 2015 to at least 2020, the AMS Collaboration decided to exchange the SuperConducting Magnet (SCM) with the AMS01 Permanent Magnet (PM). The PM has a five time lower magnetic field but an unlimited lifetime. The reduced bending power will be compensated by a different tracker planes configuration which significantly extends the lever arm of the curvature measurement outside the magnet bore. In this configuration the accuracy of the charge sign determination will be the same as with the SCM. Although this configuration decreases the AMS acceptance for high energy particles by about 40 %, the statistical accuracy is greatly compensated by the much longer exposure time.

Acknowledgments

This work could not have been carried out without the intense and dedicated effort by R. Pilastrini, F. Massera, A. Zucchini and all the technical staff of the INFN, Bologna and of M. Tesi and A. Gabbanini from CNR-IROE, Florence. Special thanks are due to the SERMS laboratory staff and to the Carlo Gavazzi Space engineers for their assistance and friendly collaboration during the space qualification tests in Terni.

References

[1] S.P. Ahlen et al., Nucl. Instrum. Methods A 350 (1994) 351.

[2] M. Aguilar et al., Phys. Rep. 366 (2002) 331.

[3] D. Bollini et al., Nuovo Cimento 61A (1969) 125.

[4] A. Zichichi, Ann. Phys. 66 (1971) 405.

[5] A. Zichichi, Elementary Processes at High Energy, Acad. Press (1971) 790.

[6] M. Basile et al., Nucl. Instrum. Methods A 179 (1981) 477.

[7] V. Bindi et al., The AMS-02 TOF electronics, in progress.

[8] L. Brocco et al., Proc. 7th ICATPP, World Scientific (arXiv:hep-ex/0111096), 2001.

[9] Hamamatsu Photonics, Photomultiplier tube RS946 (1994).

[10] M. Adinolfi et al., Nucl. Instrum. Methods A 482 (2002) 363.

[11] L. Brocco et al., Proc. 27th ICRC (2001) 2193-2196.

[12] G. Levi et al., Nucl. Instrum. Methods A 530 (2004) 419.

[13] L. Amati et al., IEEE NSS Conf. Rec. 1 (2004) 366-370.

[14] L. Amati et al., Proc. 29th ICRC 9 (2005) 45-48.

[15] D. Casadei, Ph.D. Thesis, Univ. Bologna (2003).

[16] J.B. Birks, The Theory and Practice of Scintillation Counting, Pergamon Press (1964).

[17] Alpha magnetic spectrometer-02 structural verification plan, JSC 28792, Rev. C (2003).